Constraining Extended Scalar Sectors at the LHC and beyond

Agnieszka Ilnicka

Institute of Physics, University of Zurich
Winterthurstrasse 190, CH-8057 Zurich, Switzerland
ailnicka@physik.uzh.ch

Tania Robens

MTA-DE Particle Physics Research Group, University of Debrecen
4010 Debrecen, Hungary
tania.robens@science.unideb.hu

Tim Stefaniak

Deutsches Elektronen-Synchrotron DESY
Notkestraße 85, 22607 Hamburg, Germany
tim.stefaniak@desy.de

We give a brief overview of beyond the Standard Model (BSM) theories with an extended scalar sector and their phenomenological status in the light of recent experimental results. We discuss the relevant theoretical and experimental constraints, and show their impact on the allowed parameter space of two specific models: the real scalar singlet extension of the Standard Model (SM) and the Inert Doublet Model. We emphasize the importance of the LHC measurements, both the direct searches for additional scalar bosons, as well as the precise measurements of properties of the Higgs boson of mass 125 GeV. We show the complementarity of these measurements to electroweak and dark matter observables.

Preprint number: DESY 18-031

1. Introduction

With the startup of data taking at the LHC in 2010 particle physics has entered an exciting era, with a milestone reached in 2012 with the discovery of a Higgs boson with a mass of 125 GeV.[1,2] The experimental results from the ATLAS and CMS collaborations from Run I and the currently ongoing Run II are in good agreement with the predictions of the Standard Model, in particular, the discovered Higgs particle appears to be consistent with the expectations for a SM Higgs boson.[3] However, both the experimental and theoretical uncertainties still leave room for new physics.

Extensions of the scalar sector can provide intriguing scenarios for new physics. Additional terms in the scalar potential may elicit a strong first-order electroweak phase transition [4,5,6,7,8,9], and/or provide new sources of CP violation (see e.g. Ref. 10) — both are needed if the matter-antimatter asymmetry of the Universe is generated during the electroweak phase transition.[11,12] Moreover, models with

extended scalar sectors may feature a suitable candidate for the dark matter (DM) observed in our Universe and/or scalar particle(s) that mediate the interactions of the visible to a dark sector (i.e. so-called *Higgs portal* models).[13] From the UV perspective, models with extended Higgs sectors are often obtained as an effective low-energy description of a more complete BSM theory (e.g. Supersymmetry), which in turn may address other shortcomings of the SM, e.g. the hierarchy problem or the unification of gauge couplings.[14]

In this review we discuss important phenomenological constraints that generally need to be taken into account in the investigation of models with an extended scalar sector.[a] We demonstrate these constraints on two simple models, in which the SM Higgs sector is extended by *(i)* a real scalar singlet field, and *(ii)* an inert scalar $\mathrm{SU}(2)_L$ doublet. The first model can be considered as a minimal extension of the SM with only one additional field, whereas the second model is very attractive as the lightest inert scalar boson in the model is a suitable DM candidate. A full discussion of all constraints in these models has been presented in Refs. 15, 16, 17, 18, 19, 20; here we only emphasize the most important constraints and refer the reader to the above references for a complete study.

1.1. (*i*) *Higgs singlet extension*

In the *Higgs singlet extension*, in its simplest version, the SM scalar sector is augmented by a real scalar field that is a singlet under the SM gauge group. The scalar potential can be simplified by requiring the model to be renormalizable and imposing additional symmetries. We here discuss the case where the model is symmetric under an additional Z_2 symmetry.[13,21]

Under these assumptions the scalar potential is given by

$$V(\Phi, S) = -m^2\Phi^\dagger\Phi - \mu^2 S^2 + \lambda_1(\Phi^\dagger\Phi)^2 + \lambda_2 S^4 + \lambda_3\Phi^\dagger\Phi S^2, \tag{1}$$

with the two scalar fields given by

$$\Phi \equiv \frac{1}{\sqrt{2}}\begin{pmatrix} 0 \\ \tilde{h} + v \end{pmatrix}, \qquad S \equiv \frac{h' + x}{\sqrt{2}}, \tag{2}$$

in the unitary gauge, and $\tilde{h}$ and h' being the dynamical degrees of freedom and v and x the vacuum expectation values (vevs). The kinetic term of the Lagrangian reads

$$\mathscr{L}_{s,\mathrm{kin}} = (D^\mu\Phi)^\dagger D_\mu\Phi + \partial^\mu S\partial_\mu S. \tag{3}$$

The gauge eigenstates are rotated into the mass eigenstates by a mixing angle α,

$$\begin{pmatrix} h \\ H \end{pmatrix} = \begin{pmatrix} \cos\alpha & -\sin\alpha \\ \sin\alpha & \cos\alpha \end{pmatrix}\begin{pmatrix} \tilde{h} \\ h' \end{pmatrix}. \tag{4}$$

[a]Naturally, in this brief review we cannot give a complete overview of this broad topic. We therefore confine ourselves to two simple, illustrative BSM scenarios.

Another important parameter is the ratio of the two vevs, $\tan\beta \equiv v/x$. After minimization of the scalar potential the model contains five free parameters, which can be chosen to be

$$m_h,\, m_H,\, \sin\alpha,\, \tan\beta,\, v,$$

where $m_h\,(m_H)$ denotes the mass of the lighter (heavier) mass eigenstate. Electroweak precision observables set $v \sim 246$ GeV. One of the two Higgs particles, h or H, must be identified with the Higgs particle measured by the LHC experiments with a mass of ~ 125 GeV. This leaves three free parameters, which are further constrained by theoretical and experimental constraints, as discussed below.

1.2. (*ii*) *Inert Doublet Model*

Another intriguing extension of the SM scalar sector is the *Inert Doublet Model* (IDM)[22,23,24] which features a dark matter candidate. In this two Higgs doublet model, the additional $\mathrm{SU}(2)_L$ doublet, ϕ_D, is made *inert* for the SM matter sector by imposing a discrete Z_2 symmetry, which we call D-symmetry, with the following transformation properties:

$$\phi_S \to \phi_S, \quad \phi_D \to -\phi_D, \quad \text{SM field} \to \text{SM field}. \tag{5}$$

This discrete symmetry is respected by the Lagrangian and the vacuum, i.e. ϕ_D does not acquire a vev. The other doublet, ϕ_S, on the other hand, plays the same role as the Higgs doublet in the SM, and yields a SM-like Higgs state, h. The so-called *inert* or *dark* doublet ϕ_D contains four scalar degrees of freedom that manifest as a charged scalar boson pair, $H^\pm$, and two neutral scalar bosons, H and A, with the lighter neutral inert scalar being a natural DM candidate. The potential of this model is given by

$$\begin{aligned} V(\phi_S,\phi_D) = &-\tfrac{1}{2}\left[m_{11}^2(\phi_S^\dagger\phi_S)+m_{22}^2(\phi_D^\dagger\phi_D)\right] + \tfrac{\lambda_1}{2}(\phi_S^\dagger\phi_S)^2+\tfrac{\lambda_2}{2}(\phi_D^\dagger\phi_D)^2 \\ &+\lambda_3(\phi_S^\dagger\phi_S)(\phi_D^\dagger\phi_D)+\lambda_4(\phi_S^\dagger\phi_D)(\phi_D^\dagger\phi_S) + \tfrac{\lambda_5}{2}\left[(\phi_S^\dagger\phi_D)^2+(\phi_D^\dagger\phi_S)^2\right]. \end{aligned} \tag{6}$$

After the minimization of the potential, the model has in total seven a priori free parameters

$$\underbrace{M_h,\, v}_{\phi_S},\, \underbrace{M_H,\, M_A,\, M_{H^\pm}}_{\phi_D},\, \underbrace{\lambda_2,\, \lambda_{345}}_{\text{IDM}}, \tag{7}$$

that are associated to the SM-like scalar doublet, ϕ_S, the dark scalar doublet, ϕ_D, or the scalar potential, Eq. (6), respectively. Due to the different transformation properties under the D-symmetry there is no mixing of the neutral scalar fields between the two doublets. The coupling λ_2 governs the interactions within the dark sector, while $\lambda_{345} \equiv \lambda_3+\lambda_4+\lambda_5$ is responsible for the interactions between the SM-like Higgs boson h and the DM particle. The inert doublet, ϕ_D, transforms equivalently to ϕ_S under the SM gauge group; however, due to the exact Z_2 symmetry, it does not contribute to electroweak symmetry breaking. In turn, this implies that both

v and M_h are fixed by electroweak precision observables and the mass measurement of the Higgs boson observed at the LHC. This leaves in total 5 undetermined parameters, which are subject to various theoretical and experimental constraints (see below). Choosing one of the new scalars as the DM candidate naturally implies a mass hierarchy in the inert sector. Here we chose H as DM candidate, hence $M_H \leq M_A, M_{H^\pm}$.[b]

2. Theoretical constraints

In general, all extensions of the SM are subject to a large number of theoretical and experimental constraints. Quite generally, the following conditions have to be fulfilled in order to have a reliable perturbative description of the model:

(i) the potential must be bounded from below and display at least a local (if not global) minimum;
(ii) the matrix of all $2 \to 2$ scattering processes must be unitary; this condition is imposed by making use of perturbative unitarity[25], which renders an upper limit on the coefficients of the partial wave expansion for the scattering matrix;
(iii) perturbativity of the couplings; for a coupling λ, this implies $|\lambda| \leq 4\pi$.

Conditions (i) and (iii) above directly lead to constraints on (relations of) couplings; the second condition depends on more involved relations, but can easily be implemented using numerical tools.

For the IDM, two minima can coexist, leading to an additional requirement in order to guarantee the inert vacuum to be global.[26,27,28]

3. Experimental constraints from collider experiments

A BSM theory with an extended scalar sector can only be phenomenologically viable if *(i)* it features a Higgs boson that is consistent with the observed properties of the Higgs boson signal at the LHC, and *(ii)* the remaining scalar states of the model are not in conflict with the null-results in collider searches for additional scalar states. For the latter, besides the current collider experiment (LHC) it can also be important to take limits from past collider experiments (LEP, Tevatron) into account. It is then an interesting question how these collider constraints compare to other, complementary probes for BSM effects, and what the future prospects are for a discovery/exclusion of the model.

3.1. *Searches for additional Higgs bosons*

In the real singlet extension, the couplings of the additional Higgs state to SM particles are reduced universally by the mixing angle; assuming that the lighter

[b]Note that choosing A as DM candidate, i.e. $M_A \leq M_H, M_{H^\pm}$, is phenomenologically identical to our choice, with the replacement $\lambda_{345} \longleftrightarrow \bar{\lambda}_{345} \equiv \lambda_3 + \lambda_4 - \lambda_5$ everywhere.

Higgs boson h is the discovered SM-like Higgs boson with $m_h \simeq 125$ GeV, the couplings of H to SM bosons and fermions are rescaled by $\sin\alpha$. In addition, if $m_H > 2m_h$, the additional decay mode $H \to hh$ is kinematically allowed and can be sizable. Hence, two types of LHC searches are relevant, namely, for direct Higgs production $pp \to H$ with successive decay to SM particles (mostly importantly, WW and ZZ)[29,30,31,32,33] or to a pair of SM-like Higgs bosons[34,35]. Constraints from these (and other) Higgs searches can be conveniently tested for (nearly) arbitrary BSM theories with the public tool `HiggsBounds`[36,37,38,39,40], which we also employ here.

In Fig. 1 we show a comparison of theoretical and experimental constraints on the parameters m_H and $\sin\alpha$ in the real singlet extension (for fixed $\tan\beta = 0.1$). Current LHC searches for additional Higgs bosons (*green dotted line*) provide the strongest constraint in the lower mass range (i.e., roughly, $m_H \in [130,\ 300]$). The displayed constraints are obtained from Run II ATLAS and CMS searches with WW and ZZ final states using ~ 36 fb^{-1} of collected data.[29,30,31,32,33] At higher masses, indirect constraints obtained from the W-boson mass (see Sect. 4.1) are more constraining, however, could also be alleviated more easily by new physics *beyond* the real singlet extension. Yet, the LHC direct searches remain to provide useful and robust constraints on the mixing angle even for larger m_H.

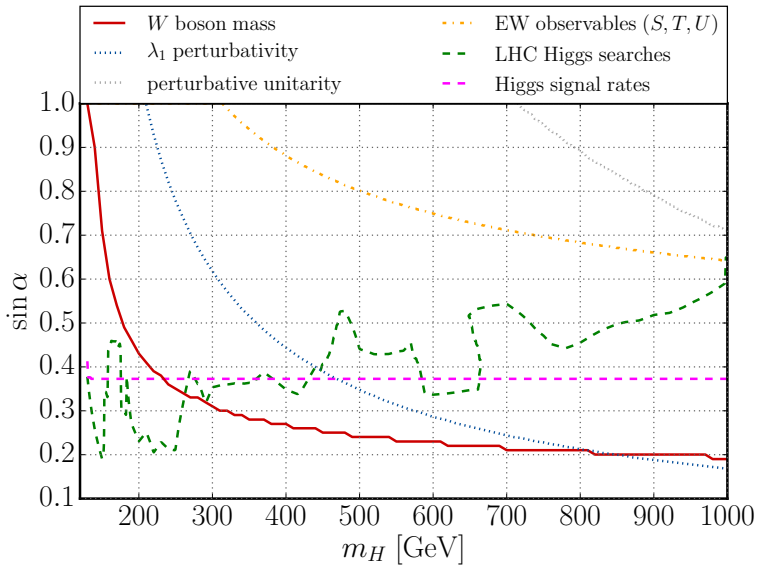

Fig. 1. Constraints on the mixing angle, $|\sin\alpha|$, as a function of the additional Higgs boson mass, m_H, in the real singlet extension of the SM (for fixed $\tan\beta = 0.1$): Theoretical constraints from perturbativity of the couplings (*dotted blue*), perturbative unitarity (*dotted gray*), and experimental constraints from the W-boson mass (*solid red*), electroweak precision observables (*dot-dashed orange*), LHC Higgs searches for additional Higgs bosons (*dashed green*) and LHC measurements of the Higgs signal rates (*dashed magenta*).

For the IDM, on the other hand, direct production of the additional (inert) scalar states is suppressed due to the Z_2 symmetry, which only allows them to be produced pair-wise. The conventional LHC searches for additional Higgs states thus do not apply straight-forwardly to the IDM. However, results from LEP and LHC searches for supersymmetric particles can be recasted to the IDM, yielding strong constraints on certain regions of parameter space. A reinterpretation of a LEP search for neutralino pair production[41] excluded a region of the IDM parameter space where

$$M_A \leq 100 \text{ GeV}, \quad M_H \leq 80 \text{ GeV} \quad \text{and} \quad \Delta M(A,H) \geq 8 \text{ GeV}, \tag{8}$$

simultaneously.[42] This limit is taken into account in the results presented here.[18]

At the LHC the searches for final states containing multi-leptons and missing transverse energy show the best sensitivity to the IDM.[43] However, Ref. 18 pointed out that the regions excluded by these searches are also subject to other constraints, e.g. from DM detection and the observed DM relic abundance.

The most promising LHC signatures in the IDM contain final states with a single or two electroweak gauge bosons, associated with a pair of DM particles which lead to missing transverse energy. Many supersymmetric searches target the same final states and are therefore ideal candidates for reinterpretation. However, the decay topologies typically differ in these two models. The event selection of supersymmetric searches is therefore not optimized for similar processes in the IDM. Hence, future experimental searches designed specifically to the IDM processes would significantly enhance the LHC discovery potential for the IDM.

3.2. *Limits from Higgs signal rates*

BSM effects can modify the signal rates of the 125 GeV Higgs boson with respect to the SM prediction in various ways, e.g.

- by directly modifying its tree-level couplings to SM particles;
- by modifying its couplings to SM particles at the loop-level. This is particularly relevant in cases where the leading SM and BSM contributions enter at the same order of perturbation theory, which is often the case for the Higgs couplings to photons and gluons;
- by introducing genuine Higgs decay channels that do not exist for the SM Higgs boson. Generically, new decay mode(s) lead to an overall suppression of the Higgs decays to SM final states.

Hence, quite generally, the LHC measurements of the Higgs signal rates provide important constraints on the BSM parameter space. These can be easily evaluated for (nearly) arbitrary BSM theories with the public code `HiggsSignals` [44] (see also Ref. 45) by means of a χ^2 test.

The two models considered here nicely demonstrate the three possible Higgs rate modifications. In the real singlet extension, the tree-level Higgs couplings to

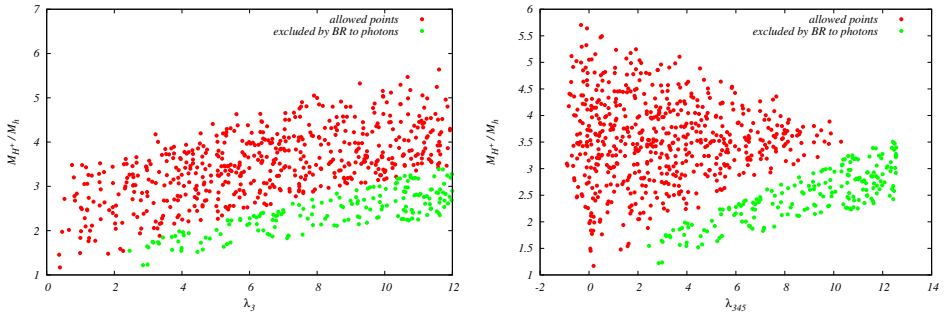

Fig. 2. Constraints on the Inert Doublet Model from the LHC Higgs signal rate for $h \to \gamma\gamma$: Points allowed (red) and excluded (green) in the $(\lambda_3, M_{H^\pm}/M_h)$ *(left)* and $(\lambda_{345}, M_{H^\pm}/M_h)$ *(right)* plane. Here we allow for under-abundant DM, such that large λ_{345} values are possible. This plot only contains points with DM masses $m_H \geq 130\,\text{GeV}$. Figure taken from Ref. 20.

SM particles is uniformly rescaled by the mixing angle (either by $\cos\alpha$ or $\sin\alpha$, depending on whether h or H is the Higgs candidate at 125 GeV). In addition, if $2m_h \leq m_H \simeq 125$ GeV, the decay channel $H \to hh$ is kinematically allowed. In contrast, in the IDM, the tree-level Higgs couplings are unmodified, however, the charged scalar boson $H^\pm$ can contribute to the Higgs-photon-photon coupling at one-loop level[46,47] (i.e., at the same order as SM contributions). Furthermore, additional decay modes of the Higgs candidate at 125 GeV to pairs of the inert scalars can be possible.

We employed `HiggsSignals` to check the Higgs signal rate constraints in the real scalar singlet extension, using the results from the ATLAS and CMS Run I combination[3] and recent Run II results[48,49,50,51,52,53,54,55]. Here, we only focus on the mass region $m_H \gtrsim 130$ GeV, with the lighter Higgs boson being the Higgs candidate at 125 GeV, where we obtain an upper limit of $|\sin\alpha| \lesssim 0.37$ at 95% confidence level (C.L.), see Fig. 1. For the lower mass range, and in particular the inverted case with H at 125 GeV, it is important to take into account a potential signal overlap of both Higgs bosons, as well as the additional decay mode $H \to hh$.[c]

For the Inert Doublet Model the numerical results presented here[18,20] employ the public code `2HDMC`[56] to obtain the Higgs sector predictions. In particular, this includes the branching ratio predictions for the invisible Higgs decay, $\text{BR}(h \to HH)$, and the loop-induced Higgs to diphoton decay, $\text{BR}(H \to \gamma\gamma)$, which receives contributions from the inert charged scalar boson. The parameters relevant for this loop-induced process are λ_3 and the ratio M_{H^+}/M_h, which are shown in Fig. 2 (*left*). As can be seen, the Higgs rate measurements yield a clear exclusion in the lower right corner, i.e. for large λ_3 and small ratios M_{H^+}/M_h. Similarly, due to the linear connection between λ_3 and λ_{345}, we obtain a clear discrimination between

[c]These cases are discussed in detail in Ref. 17. Note also that for the parameter constellation $\tan\beta = -\cot\alpha$ the decay rate for $H \to hh$ vanishes independent of the masses.

allowed and excluded regions in the input parameter plane (λ_{345}, M_{H^+}/M_h), see Fig. 2 (*right*).

The parameter region with $M_H \leq M_h/2$ is very sensitive to branching ratio limits for the invisible decay of the SM-like Higgs boson. This constraint alone already yields the limit $|\lambda_{345}| \lesssim 0.02$ in this mass range, see Fig. 3. In this result we used rate measurements from the ATLAS and CMS Run I combination.[3]

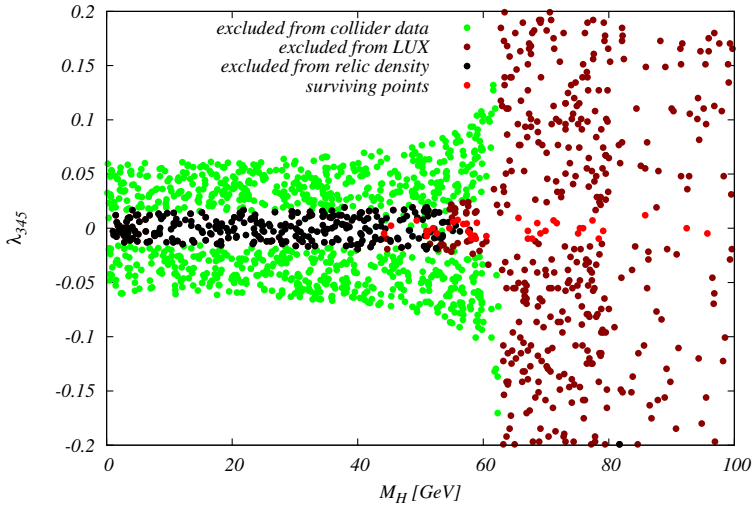

Fig. 3. Comparison of constraints in the Inert Doublet Model in the (M_H, λ_{345}) plane for low DM masses: We show parameter points excluded by collider data, i.e. the limit on the invisible decay rate of the SM-like Higgs boson inferred from the ATLAS and CMS combined Run 1 results in *green*. Direct DM detection searches and DM relic abundance (see Sect. 4.2) exclude the points shown in *brown* and *black*, respectively. The points surviving all constraints are shown in *red*. Figure taken from Ref. 20.

4. Other constraints

Besides the collider constraints from Higgs searches and measurements, as discussed above, both models are subject to additional constraints. The most important ones, namely the constraints from electroweak precision observables (EWPOs) and, in case of the IDM, from DM observables, will be discussed separately below. We further want to mention that limits on the total decay width of the 125 GeV Higgs boson (with current value $\Gamma_{\text{tot}} \leq 13$ MeV 57), as well as the total decay widths of the electroweak gauge bosons, could give rise to additional constraints. Moreover, in the IDM restrictions arise from long-lived charged particle searches at the LHC in the case of almost degenerate masses between the inert charged scalar boson and the DM candidate, discussed in detail in Ref. 58. Further model-specific limits are

discussed in Ref. 18.

4.1. *Electroweak precision observables*

A standard way to check constraints from electroweak precision observables (EWPOs) in new physics models is to entertain the so-called oblique parameters, where the most relevant variables are the S, T, U parameters.[59,60,61,62] The constraints from S, T and U can be implemented by evaluating

$$\chi^2_{\rm STU} = \mathbf{x}^T \mathbf{C}^{-1} \mathbf{x}, \tag{9}$$

with $\mathbf{x}^T = (S - \hat{S}, T - \hat{T}, U - \hat{U})$, where the central values $\hat{S}, \hat{T}, \hat{U}$, as well as the covariance matrix $\mathbf{C}$ are provided by a global fit to the EWPOs.[63,64] Requiring $\chi^2_{\rm STU} \leq 8.025$ corresponds to a maximal 2σ deviation given the three statistical degrees of freedom.

We have applied this procedure to both models. In the real singlet extension, however, the derived bound from EWPOs are always superseded by other stronger constraints. In the IDM, as can be inferred from Fig. 4, the EWPOs do impose notable constraints in the parameter space. However, a clear separation of allowed and excluded regions in the shown two-dimensional projected parameter planes cannot be identified.

Another way to constrain new physics models from the electroweak sector is to calculate specific observables that are highly sensitive to new physics contributions. A prime example for this is the mass of the W-boson. Here, the current experimental world-average value is given by[65]

$$m_W^{\rm exp} \;=\; (80.315 \,\pm\, 0.015)\,\text{GeV}. \tag{10}$$

In Ref. 16 the consequences of using the W-boson mass as a stand-alone constraint were investigated in the framework of the real singlet extension. For the case where $m_H \;\geq\; 125\,\text{GeV}$, this indeed leads to strong limits on the allowed range for $\sin\alpha$

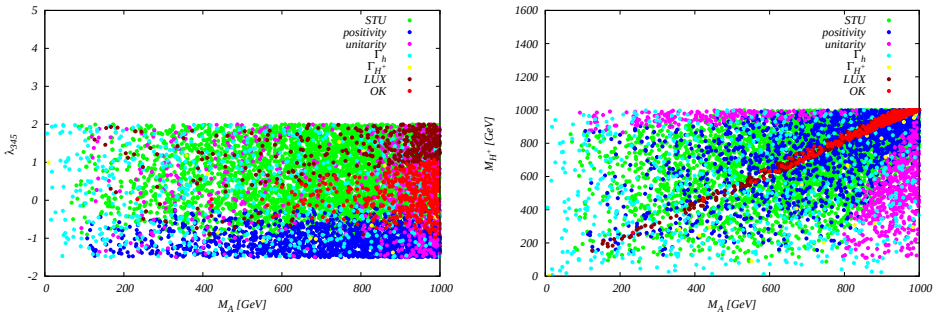

Fig. 4. Combined constraints in two exemplary 2D parameter projections in the Inert Doublet Model. The colored points represent parameter points that were excluded by the individual constraints, which are applied in the same order as named in the legend. Allowed points are displayed in red; *left:* $(M_A,\ \lambda_{345})$ plane, *right:* $(M_A, M_{H^\pm})$ plane. Figure taken from Ref. 18.

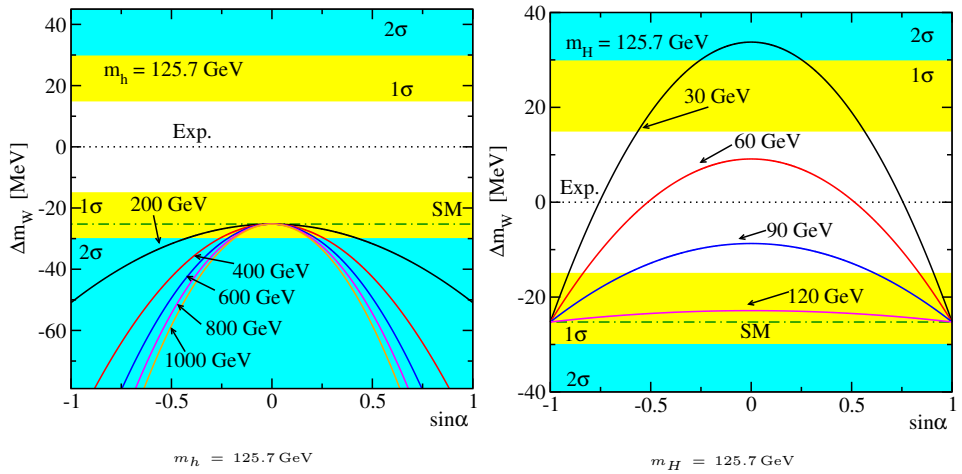

Fig. 5. Dependence of Δm_W, as defined in Eq. (11), on the mixing angle $\sin\alpha$ for cases where the lighter *(left)* or heavier *(right)* scalar boson corresponds to the 125 GeV Higgs state, for different values of the additional scalar boson mass. Figure taken from Ref. 16.

(see Fig. 1). The main reason for the strength of this constraint is the current discrepancy between the experimental value, Eq. (10), and the SM prediction of 80.360 GeV.[66] The $\sin\alpha$ dependence of the discrepancy,

$$\Delta\, m_W \;\equiv\; m_W^{\text{singlet}} - m_W^{\text{exp}}, \tag{11}$$

is shown in Figure 5 for various values of the additional scalar boson mass. In the scenario where $m_h \simeq 125$ GeV, higher-order electroweak corrections increase the discrepancy between the BSM prediction and the experimental value, therefore leading to strong constraints when requiring agreement with the experimental value on a 2σ level. On the other hand, for $m_H \simeq 125$ GeV, the corrections are able to reconcile the measurement with the theory prediction in certain regions of the parameter space. However, in this case Higgs signal rate measurements and direct searches at LEP strongly constrain the mixing angle to values $|\sin\alpha| \approx 1$.[17,19]

In summary, electroweak precision observables pose important constraints on new physics scenarios with extended scalar sectors. In particular, in cases where they further increase the discrepancy between SM prediction and observed value for specific observables, as e.g. the W-boson mass, they can render the most stringent limits in large regions of parameter space.

4.2. *Dark matter constraints*

For models with a dark matter candidate, constraints from DM observables need to be taken into account (see e.g. Ref. 67). The most important are the following:

- The DM relic density produced by the model should not overclose the Universe.

This leads to requiring an upper limit for the cold DM relic abundance of

$$\Omega_c h^2 \leq 0.1241, \tag{12}$$

corresponding to the 2σ allowed upper value from the Planck collaboration[68]. Note that, by imposing only the upper limit on $\Omega_c h^2$, we do allow for DM to be under-abundant.

- Limits from DM direct detection experiments. In Ref. 18 values from the LUX experiment[69] were taken into account; results using updated experimental limits from LUX[70] were presented in Ref. 20. In this review, we present updated results using the latest constraints from the Xenon1T experiment[71].[d]
- Limits from DM indirect detection experiments. Most recent bounds stem from SuperKamiokande (see e.g. Refs. 73, 74), Icecube[75], and Fermi-LAT[76] for $b\bar{b}$, $\tau\,\tau$, $W^+\,W^-$, and photonic final states, respectively. We did not include these in the results presented here.[e]

Predictions for the DM observables in the IDM were obtained using micrOMEGAs[78], assuming a standard cosmological thermal history.

The impact of the DM constraints is quite different for DM candidates with high and low mass values.[f] We will therefore discuss them separately.

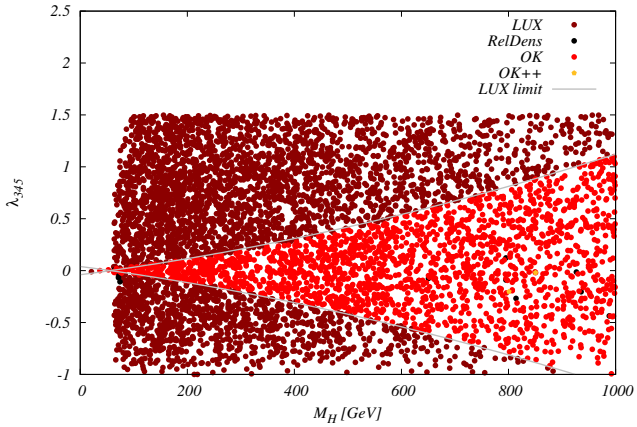

Fig. 6. Constraints on the Inert Doublet Model in the (M_H, λ_{345}) plane from DM direct detection experiments: Bright red points are allowed and dark red points are excluded. Additionally, points that reproduce the observed relic density are marked in gold (OK++). Figure taken from Ref. 18.

In general, the two IDM parameters which are most sensitive to limits from direct

[d]We employ the digitized data from Ref. 72 in this work.
[e]See e.g. Ref. 77 for a recent fit study incorporating indirect detection constraints.
[f]Many of the results discussed here are IDM specific. However, they serve to demonstrate the complementarity of collider searches and astrophysical observations, and can be instructive for the investigation of other BSM dark matter scenarios, especially with a Higgs portal to the DM sector.

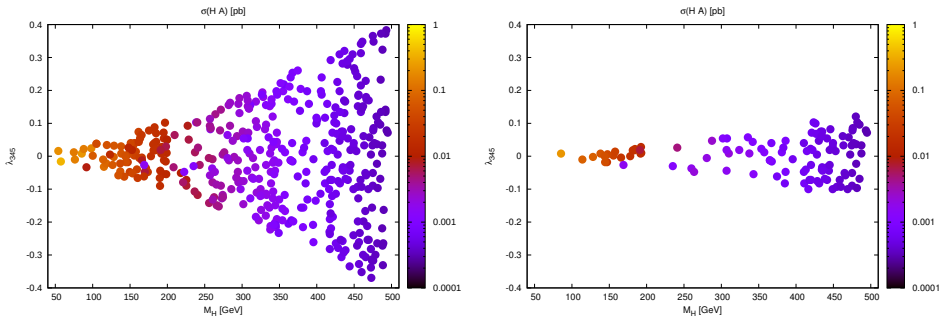

Fig. 7. Production cross section (in pb) for $pp \to HA$ production at the 13 TeV LHC in the Inert Doublet Model, after applying the LUX *(left)* and XENON1T *(right)* DM direct detection constraints. The allowed parameter space shrinks considerably once the newer experimental bounds are taken into account. The left figure is taken from Ref. 18.

detection experiments are the dark matter mass, M_H, as well as the coupling λ_{345}. As an example, Fig. 6 show the constraints on these parameters (Fig. taken from Ref. 18). It illustrates that in particular for the mass range $M_H \gtrsim M_h/2$ the LUX limit clearly separates the parameter space. Newer direct detection results improve the limits by an order of magnitude. This is exemplarily shown in Fig. 7, displaying the production cross section for $pp \to HA$ — one of the dominant production modes of the IDM at hadron colliders[18,79] — at the 13 TeV LHC for regions allowed after applying LUX *(left)* and 2017 XENON1T *(right)* DM direct detection limits. These updated constraints lead to a significant decrease of the allowed parameter regions. The production cross sections were calculated using `Madgraph-5`[80], using a UFO model file for the IDM from Ref. 81.

For low DM masses, in particular the case $M_H \leq M_h/2$, constraints from the LHC Higgs signal strengths play an important role, as the new decay mode $h \to HH$ of the observed Higgs boson becomes kinematically accessible (see Sect. 3.2). However, as can be seen from Figure 3, the most stringent bounds in this region stem from relic density constraint, Eq. (12). Here, large relic density values are obtained from the predominant annihilation channels $HH \to b\bar{b}$ and $HH \to hh$, see Refs. 81, 18, 82. The resulting parameter space, after including the latest XENON1T limits, is shown in Figure 8. The DM relic density limit prevails in most regions of the parameter space; in combination with direct detection limits, this leads to $|\lambda_{345}| \lesssim 0.01$ for $M_H \leq M_h/2$. Let us emphasise, that the gain in sensitivity between LUX and XENON1T lead to a decrease of allowed values for this coupling by a factor two with respect to the results presented in Ref. 18.

As discussed above, astrophysical constraints mainly affect the coupling λ_{345} in the IDM. On the other hand, production and decay processes at the LHC are dominantly determined by the masses of the inert scalars and the SM electroweak

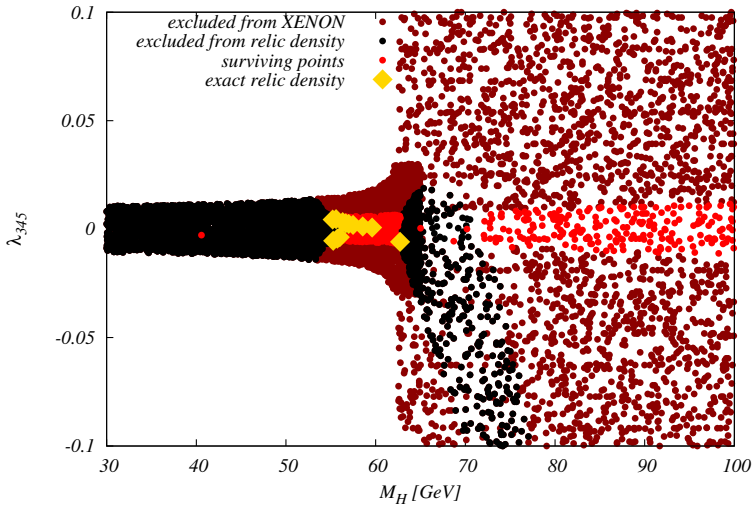

Fig. 8. Comparison of dark matter constraints in the Inert Doublet Model in the (M_H, λ_{345}) parameter plane for low DM masses. Parameter points excluded by the latest XENON1T limit or the DM relic density are shown in *brown* and *black*, respectively. Allowed points are shown in *red*, and *yellow* points correspond to scenarios that exactly reproduce the DM relic density within 95 % C.L..

couplings.[18] Therefore, the IDM is a prime example for a model that features an important complementarity between dark matter and collider searches. In fact, recent developments in the field of DM direct detection experiments will hopefully allow to further constrain or discover this model in the near future.[83]

5. Conclusions

We briefly reviewed theoretical and experimental constraints that need to be taken into account when considering models with extended scalar sectors. For illustration, we discussed two simple Beyond the Standard Model scenarios: First, the real scalar singlet extension of the Standard Model, and second, the Inert Doublet Model, i.e. a two Higgs doublet model featuring a dark matter candidate. While direct LHC searches for additional scalar states, as well as the measurement of the 125 GeV Higgs boson signal strengths, limit the models' parameter space significantly, we also pointed to the importance of complimentary limits from other areas, with a focus on electroweak precision observables and dark matter constraints. In summary, BSM scenarios with extended scalar sectors can be probed in various ways, and we hope that the near future will bring a discovery either directly in collider or dark matter searches, or indirectly through precision measurements (or both).

Acknowledgments

TR wants to thank G.M. Pruna, D. Lopez-Val, and G. Chalons for fruitful collaboration on related topics. This material is based in part upon work supported by part by the National Science Centre, Poland, the HARMONIA project under contract UMO-2015/18/M/ST2/00518 (2016-2019), the National Science Foundation under Grant No. 1519045, by Michigan State University through computational resources provided by the Institute for Cyber-Enabled Research, and by grant K 125105 of the National Research, Development and Innovation Fund in Hungary. AI is supported by the 7th Framework Programme of the European Commission through the Initial Training Network HiggsTools PITN-GA-2012-316704. TS acknowledges support from the DESY Fellowship programme.

References

1. Georges Aad et al. Observation of a new particle in the search for the Standard Model Higgs boson with the ATLAS detector at the LHC. *Phys. Lett.*, B716:1–29, 2012.
2. Serguei Chatrchyan et al. Observation of a new boson at a mass of 125 GeV with the CMS experiment at the LHC. *Phys. Lett.*, B716:30–61, 2012.
3. Georges Aad et al. Measurements of the Higgs boson production and decay rates and constraints on its couplings from a combined ATLAS and CMS analysis of the LHC pp collision data at $\sqrt{s} = 7$ and 8 TeV. *JHEP*, 08:045, 2016.
4. A. I. Bochkarev, S. V. Kuzmin, and M. E. Shaposhnikov. Electroweak baryogenesis and the Higgs boson mass problem. *Phys. Lett.*, B244:275–278, 1990.
5. Neil Turok and John Zadrozny. Electroweak baryogenesis in the two doublet model. *Nucl. Phys.*, B358:471–493, 1991.
6. David Land and Eric D. Carlson. Two stage phase transition in two Higgs models. *Phys. Lett.*, B292:107–112, 1992.
7. James M. Cline, Kimmo Kainulainen, and Axel P. Vischer. Dynamics of two Higgs doublet CP violation and baryogenesis at the electroweak phase transition. *Phys. Rev.*, D54:2451–2472, 1996.
8. James M. Cline and Pierre-Anthony Lemieux. Electroweak phase transition in two Higgs doublet models. *Phys. Rev.*, D55:3873–3881, 1997.
9. A. B. Lahanas, V. C. Spanos, and Vasilios Zarikas. Charge asymmetry in two-Higgs doublet model. *Phys. Lett.*, B472:119, 2000.
10. G. C. Branco, P. M. Ferreira, L. Lavoura, M. N. Rebelo, Marc Sher, and Joao P. Silva. Theory and phenomenology of two-Higgs-doublet models. *Phys. Rept.*, 516:1–102, 2012.
11. David E. Morrissey and Michael J. Ramsey-Musolf. Electroweak baryogenesis. *New J. Phys.*, 14:125003, 2012.
12. Thomas Konstandin. Quantum Transport and Electroweak Baryogenesis. *Phys. Usp.*, 56:747–771, 2013. [Usp. Fiz. Nauk183,785(2013)].
13. Brian Patt and Frank Wilczek. Higgs-field portal into hidden sectors. 2006.
14. John F. Gunion, Howard E. Haber, Gordon L. Kane, and Sally Dawson. The Higgs Hunter's Guide. *Front. Phys.*, 80:1–404, 2000.
15. Giovanni Marco Pruna and Tania Robens. The Higgs Singlet extension parameter space in the light of the LHC discovery. *Phys.Rev.*, D88:115012, 2013.
16. D. Lopez-Val and T. Robens. Delta r and the W-boson mass in the Singlet Extension of the Standard Model. *Phys.Rev.*, D90:114018, 2014.

17. Tania Robens and Tim Stefaniak. Status of the Higgs Singlet Extension of the Standard Model after LHC Run 1. *Eur. Phys. J.*, C75(3):104, 2015.
18. Agnieszka Ilnicka, Maria Krawczyk, and Tania Robens. Inert Doublet Model in light of LHC Run I and astrophysical data. *Phys. Rev.*, D93(5):055026, 2016.
19. Tania Robens and Tim Stefaniak. LHC Benchmark Scenarios for the Real Higgs Singlet Extension of the Standard Model. *Eur. Phys. J.*, C76(5):268, 2016.
20. Agnieszka Ilnicka, Maria Krawczyk, Tania Robens, and Dorota Sokolowska. IDM and not only. *PoS*, CORFU2016:030, 2017.
21. Robert Schabinger and James D. Wells. A Minimal spontaneously broken hidden sector and its impact on Higgs boson physics at the large hadron collider. *Phys.Rev.*, D72:093007, 2005.
22. Nilendra G. Deshpande and Ernest Ma. Pattern of Symmetry Breaking with Two Higgs Doublets. *Phys. Rev.*, D18:2574, 1978.
23. Qing-Hong Cao, Ernest Ma, and G. Rajasekaran. Observing the Dark Scalar Doublet and its Impact on the Standard-Model Higgs Boson at Colliders. *Phys. Rev.*, D76:095011, 2007.
24. Riccardo Barbieri, Lawrence J. Hall, and Vyacheslav S. Rychkov. Improved naturalness with a heavy Higgs: An Alternative road to LHC physics. *Phys.Rev.*, D74:015007, 2006.
25. Benjamin W. Lee, C. Quigg, and H.B. Thacker. Weak Interactions at Very High-Energies: The Role of the Higgs Boson Mass. *Phys.Rev.*, D16:1519, 1977.
26. I.F. Ginzburg, K.A. Kanishev, M. Krawczyk, and D. Sokolowska. Evolution of Universe to the present inert phase. *Phys.Rev.*, D82:123533, 2010.
27. Michael Gustafsson. The Inert Doublet Model and Its Phenomenology. *PoS*, CHARGED2010:030, 2010.
28. Bogumila Swiezewska. Yukawa independent constraints for two-Higgs-doublet models with a 125 GeV Higgs boson. *Phys.Rev.*, D88(5):055027, 2013.
29. CMS Collaboration. Combination of standard model Higgs boson searches and measurements of the properties of the new boson with a mass near 125 GeV. 2012. CMS-PAS-HIG-12-045.
30. CMS Collaboration. Update on the search for the standard model Higgs boson in pp collisions at the LHC decaying to W + W in the fully leptonic final state. 2013. CMS-PAS-HIG-13-003.
31. Vardan Khachatryan et al. Search for a Higgs boson in the mass range from 145 to 1000 GeV decaying to a pair of W or Z bosons. *JHEP*, 10:144, 2015.
32. CMS Collaboration. Search for a new scalar resonance decaying to a pair of Z bosons in proton-proton collisions at $\sqrt{s} = 13$ TeV. 2017. CMS-PAS-HIG-17-012.
33. Morad Aaboud et al. Search for heavy ZZ resonances in the $\ell^+\ell^-\ell^+\ell^-$ and $\ell^+\ell^-\nu\bar{\nu}$ final states using proton proton collisions at $\sqrt{s} = 13$ TeV with the ATLAS detector. 2017.
34. Georges Aad et al. Search For Higgs Boson Pair Production in the $\gamma\gamma b\bar{b}$ Final State using pp Collision Data at $\sqrt{s} = 8$ TeV from the ATLAS Detector. *Phys. Rev. Lett.*, 114(8):081802, 2015.
35. Vardan Khachatryan et al. Search for two Higgs bosons in final states containing two photons and two bottom quarks in proton-proton collisions at 8 TeV. *Phys. Rev.*, D94(5):052012, 2016.
36. Philip Bechtle, Oliver Brein, Sven Heinemeyer, Georg Weiglein, and Karina E. Williams. HiggsBounds: Confronting Arbitrary Higgs Sectors with Exclusion Bounds from LEP and the Tevatron. *Comput. Phys. Commun.*, 181:138, 2010.
37. Philip Bechtle, Oliver Brein, Sven Heinemeyer, Georg Weiglein, and Karina E.

Williams. HiggsBounds 2.0.0: Confronting Neutral and Charged Higgs Sector Predictions with Exclusion Bounds from LEP and the Tevatron. *Comput. Phys. Commun.*, 182:2605, 2011.
38. Philip Bechtle, Oliver Brein, Sven Heinemeyer, Oscar Stål, Tim Stefaniak, et al. Recent Developments in HiggsBounds and a Preview of HiggsSignals. *PoS*, CHARGED2012:024, 2012.
39. Philip Bechtle, Oliver Brein, Sven Heinemeyer, Oscar Stål, Tim Stefaniak, et al. HiggsBounds-4: Improved Tests of Extended Higgs Sectors against Exclusion Bounds from LEP, the Tevatron and the LHC. *Eur. Phys. J. C*, 74:2693, 2013.
40. Philip Bechtle, Sven Heinemeyer, Oscar Stal, Tim Stefaniak, and Georg Weiglein. Applying Exclusion Likelihoods from LHC Searches to Extended Higgs Sectors. *Eur. Phys. J.*, C75(9):421, 2015.
41. M. Espirito Santo, K. Hultqvist, P. Johansson, and A. Lipniacka. Search for neutralino pair production at s**(1/2) from 192-GeV to 208-GeV. 2003.
42. Erik Lundstrom, Michael Gustafsson, and Joakim Edsjo. The Inert Doublet Model and LEP II Limits. *Phys.Rev.*, D79:035013, 2009.
43. Genevieve Belanger, Beranger Dumont, Andreas Goudelis, Bjorn Herrmann, Sabine Kraml, and Dipan Sengupta. Dilepton constraints in the Inert Doublet Model from Run 1 of the LHC. *Phys. Rev.*, D91(11):115011, 2015.
44. Philip Bechtle, Sven Heinemeyer, Oscar Stål, Tim Stefaniak, and Georg Weiglein. *HiggsSignals*: Confronting arbitrary Higgs sectors with measurements at the Tevatron and the LHC. *Eur.Phys.J.*, C74:2711, 2014.
45. Philip Bechtle, Sven Heinemeyer, Oscar Stål, Tim Stefaniak, and Georg Weiglein. Probing the Standard Model with Higgs signal rates from the Tevatron, the LHC and a future ILC. *JHEP*, 1411:039, 2014.
46. Abdesslam Arhrib, Rachid Benbrik, and Naveen Gaur. $H \to \gamma\gamma$ in Inert Higgs Doublet Model. *Phys.Rev.*, D85:095021, 2012.
47. Bogumila Swiezewska and Maria Krawczyk. Diphoton rate in the inert doublet model with a 125 GeV Higgs boson. *Phys.Rev.*, D88(3):035019, 2013.
48. Measurements of the Higgs boson production cross section via Vector Boson Fusion and associated WH production in the $WW^* \to \ell\nu\ell\nu$ decay mode with the ATLAS detector at $\sqrt{s} = 13$ TeV. *ATLAS-CONF-2016-112*, 2016.
49. Study of the Higgs boson properties and search for high-mass scalar resonances in the $H \to ZZ^* \to 4\ell$ decay channel at $\sqrt{s} = 13$ TeV with the ATLAS detector. *ATLAS-CONF-2016-079*, 2016.
50. Search for the Standard Model Higgs boson produced in association with a vector boson and decaying to a $b\bar{b}$ pair in pp collisions at 13 TeV using the ATLAS detector. *ATLAS-CONF-2016-091*, 2016.
51. Search for the Standard Model Higgs boson produced in association with top quarks and decaying into $b\bar{b}$ in pp collisions at $\sqrt{s} = 13$ TeV with the ATLAS detector. *ATLAS-CONF-2016-080*, 2016.
52. Measurement of fiducial, differential and production cross sections in the $H \to \gamma\gamma$ decay channel with 13.3 fb^{-1} of 13 TeV proton-proton collision data with the ATLAS detector. *ATLAS-CONF-2016-067*, 2016.
53. Search for the Associated Production of a Higgs Boson and a Top Quark Pair in Multilepton Final States with the ATLAS Detector. *ATLAS-CONF-2016-058*, 2016.
54. Albert M Sirunyan et al. Measurements of properties of the Higgs boson decaying into the four-lepton final state in pp collisions at $\sqrt{s} = 13$ TeV. *JHEP*, 11:047, 2017.
55. Updated measurements of Higgs boson production in the diphoton decay channel at $\sqrt{s} = 13$ TeV in pp collisions at CMS. *CMS-PAS-HIG-16-020*, 2016.

56. David Eriksson, Johan Rathsman, and Oscar Stal. 2HDMC: Two-Higgs-Doublet Model Calculator Physics and Manual. *Comput.Phys.Commun.*, 181:189–205, 2010.
57. Vardan Khachatryan et al. Search for Higgs boson off-shell production in proton-proton collisions at 7 and 8 TeV and derivation of constraints on its total decay width. *JHEP*, 09:051, 2016.
58. Alexander Belyaev, Giacomo Cacciapaglia, Igor P. Ivanov, Felipe Rojas-Abatte, and Marc Thomas. Anatomy of the Inert Two Higgs Doublet Model in the light of the LHC and non-LHC Dark Matter Searches. *Phys. Rev.*, D97(3):035011, 2018.
59. Guido Altarelli and Riccardo Barbieri. Vacuum polarization effects of new physics on electroweak processes. *Phys. Lett. B*, 253:161, 1991.
60. Michael E. Peskin and Tatsu Takeuchi. A New constraint on a strongly interacting Higgs sector. *Phys.Rev.Lett.*, 65:964–967, 1990.
61. Michael E. Peskin and Tatsu Takeuchi. Estimation of oblique electroweak corrections. *Phys.Rev.*, D46:381–409, 1992.
62. I. Maksymyk, C.P. Burgess, and David London. Beyond S, T and U. *Phys.Rev.*, D50:529–535, 1994.
63. M. Baak et al. The global electroweak fit at NNLO and prospects for the LHC and ILC. *Eur.Phys.J.*, C74(9):3046, 2014.
64. A. B. Arbuzov, M. Awramik, M. Czakon, A. Freitas, M. W. Grunewald, Klaus Monig, S. Riemann, and T. Riemann. ZFITTER: A Semi-analytical program for fermion pair production in e+ e- annihilation, from version 6.21 to version 6.42. *Comput. Phys. Commun.*, 174:728–758, 2006.
65. C. Patrignani et al. Review of Particle Physics. *Chin. Phys.*, C40(10):100001, 2016.
66. M. Awramik, M. Czakon, A. Freitas, and G. Weiglein. Precise prediction for the W boson mass in the standard model. *Phys.Rev.*, D69:053006, 2004.
67. Stefano Profumo. *An Introduction to Particle Dark Matter*. World Scientific, 2017.
68. P.A.R. Ade et al. Planck 2015 results. XIII. Cosmological parameters. 2015.
69. D.S. Akerib et al. First results from the LUX dark matter experiment at the Sanford Underground Research Facility. *Phys.Rev.Lett.*, 112(9):091303, 2014.
70. D. S. Akerib et al. Results from a search for dark matter in the complete LUX exposure. *Phys. Rev. Lett.*, 118(2):021303, 2017.
71. E. Aprile et al. First Dark Matter Search Results from the XENON1T Experiment. *Phys. Rev. Lett.*, 119(18):181301, 2017.
72. Alexander Belyaev, James Blandford, and Daniel Locke. Phenodata database. https://hepmdb.soton.ac.uk/phenodata, Jan. 2017.
73. http://lpsc.in2p3.fr/mayet/dm.php.
74. K. Choi et al. Search for neutrinos from annihilation of captured low-mass dark matter particles in the Sun by Super-Kamiokande. *Phys. Rev. Lett.*, 114(14):141301, 2015.
75. M. G. Aartsen et al. Measurement of the ν_μ energy spectrum with IceCube-79. *Eur. Phys. J.*, C77(10):692, 2017.
76. A. Albert et al. Searching for Dark Matter Annihilation in Recently Discovered Milky Way Satellites with Fermi-LAT. *Astrophys. J.*, 834(2):110, 2017.
77. Benedikt Eiteneuer, Andreas Goudelis, and Jan Heisig. The inert doublet model in the light of Fermi-LAT gamma-ray data: a global fit analysis. *Eur. Phys. J.*, C77(9):624, 2017.
78. G. Belanger, F. Boudjema, A. Pukhov, and A. Semenov. micrOMEGAs_3: A program for calculating dark matter observables. *Comput. Phys. Commun.*, 185:960–985, 2014.
79. D. de Florian et al. Handbook of LHC Higgs Cross Sections: 4. Deciphering the Nature of the Higgs Sector. 2016.
80. Johan Alwall, Michel Herquet, Fabio Maltoni, Olivier Mattelaer, and Tim Stelzer.

MadGraph 5 : Going Beyond. *JHEP*, 1106:128, 2011.
81. A. Goudelis, B. Herrmann, and O. Stal. Dark matter in the Inert Doublet Model after the discovery of a Higgs-like boson at the LHC. *JHEP*, 1309:106, 2013.
82. D. Dercks and T. Robens. in preparation.
83. Marco Battaglieri et al. US Cosmic Visions: New Ideas in Dark Matter 2017: Community Report. 2017.